Traveling-Wave Tube Nanosecond Pulse Generator in 24-Gc Region*

KAZUHIRO MIYAUCHI†

Summary—A 24-Gc traveling-wave tube of the type ECL-1180/24W80 was used for generating nanosecond carrier pulses.

The helix of the traveling-wave tube was modulated by a 40-Mc high voltage sine wave. Duration, power and carrier frequency shift of the output RF pulse were examined quantitatively with respect to the modulating voltage. It was found that the delay time of a traveling-wave tube has a large effect on the characteristics of the output pulse. The theory of transmission line modulators was developed to explain the pulse shaping mechanism in the traveling-wave tube.

Observations of output pulses were made with three measuring devices, *i.e.*, video-sampling oscilloscope with crystal detector, interferometer, and spectrum analyzer. The interferometer was found to be useful for measuring half-amplitude duration of carrier pulse.

Output pulses with half-amplitude duration of as short as 1 nsec were observed.

Introduction

TRAVELING-WAVE tube pulse generators with helix gating have been used for generating nanosecond carrier pulses by W. A. Klute [1], A. C. Beck [2] and others [3], [4]. This paper describes some of the experimental results of a pulse generator of the same construction. For this experiment the 24-Gc frequency region was used. A helix-type traveling-wave tube ECL-1180/24W80, designed for the operation in this frequency region, was employed [8].

A high voltage sinusoidal wave with frequency of 40 Mc was applied to the helix. The beam-focusing electrode was optionally modulated with the same frequency. Duration, power and carrier frequency shift of the generated carrier pulses were measured as a function of helix modulating voltage. The experimental results were compared with the theory of pulse generation mechanism described in [1]. Considerable discrepancy was observed between the theory and the experiment.

The decrease of mean power of the generated pulses with increasing helix modulating voltage was more than the expected theoretical value. This discrepancy can be explained if we take into account the transmission delay time of the microwave signal along the helix in the traveling-wave tube. The traveling-wave tube as a modulator has different characteristics than conventional modulating devices.

While it may be assumed that the modulating signal is applied instantaneously to the carrier in the latter case, the effect of modulation on the microwave carrier cannot be considered instantaneous in the former case, because it takes a finite period for the microwave signal to propagate along the helix of the traveling-wave tube. The phase relation between the modulating signal and the modulated microwave signal varies along the helix.

This variation of the phase relation along the helix causes a type of modulation distortion and decreases the duration and the power of the output pulse. This type of modulation distortion was analyzed in the general case. A modulator in which the carrier is modulated along a transmission line with time-varying parameters is called "transmission line modulator" in this paper. It was found that transmission line equations in the transmission line modulator are reduced to Lagrange's linear equations and easily solved.

The mean power of the generated pulse train was calculated in terms of helix gating duration by this theory. Considerable agreement was observed between the calculated and experimental results.

The present analysis of the transmission line modulator has some applications. It can be applied not only to the traveling-wave tube pulse generator with helix gating, but also to the traveling-wave tube phase modulator with helix modulation or traveling-wave tube amplitude modulator with beam-focusing electrode modulation. These applications are briefly discussed in this paper.

The generated pulses were observed with three measuring devices: video-sampling oscilloscope with crystal detector, waveguide interferometer, and spectrum analyzer.

The characteristics of these devices are explained briefly in this paper. It was found that the interferometer with peak detector is applicable when measuring the half-amplitude duration of the carrier pulses with a constant repetition rate. RF pulses with half-amplitude duration of as short as 1 nsec were observed with these measuring devices.

Mechanism of Pulse Shaping

When we consider a traveling-wave tube whose helix voltage is swept with an extremely fast increasing or decreasing voltage, it must be noticed that the modulation voltage is not constant over the period required for the microwave signal to propagate through the traveling-wave tube.

Here it will be assumed that the modulation voltage is applied to each point of the helix with a common time variation, and that the modulation characteristic is

* Received June 8, 1962; revised manuscript received August 24, 1962.

† Electrical Communication Laboratory, Nippon Telegraph and Telephone Public Corporation, Tokyo, Japan.

uniform along the helix. Then, an equivalent circuit of the helix-modulated traveling-wave tube as illustrated in Fig. 1 is obtained. M_1, M_2, $\cdots$, M_{n+1} are partial modulators operating with a common time variation and without internal signal delay, and T_g is the signal delay time through the traveling-wave tube. The number of partial modulators $n+1$ is assumed sufficiently large.

A considerable amount of modulation distortion is caused by the presence of T_g when it is not small. Fig. 2 (a) and (b) illustrate some models of the modulator with $n=2$ to see how the modulation distortion results from the helix delay time T_g.

In Fig. 2 (a), the output of each partial modulator is confined within a certain duration Te. Hence, the base width of modulation pattern or output pulse can be defined. The modulator input is assumed to be a continuous wave of unit amplitude. If the delay time is not present ($T_g=0$), the output waveform of the modulator will be the product of modulating waveforms of three partial modulators. The resulting output waveform is illustrated in Fig. 2 (a)-(iv). If the delay time is present ($T_g \neq 0$), considerably different results are obtained as illustrated in Figs. 2(a)-(i), (ii) and (iii). The input waveforms of the partial modulators M_2 and M_3 are delayed by a delay time $T_g/2$ with respect to the output waveforms of the partial modulators M_1 and M_2, respectively. Curve ② in Fig. 2(a)-(iii) denotes the resulting output waveform of the modulator.

Waveform, peak amplitude and duration of the curve ② in Fig. 2(a)-(iii) are apparently different from these of the curve in Fig. 2(a)-(iv). It is easily seen that the base width and the peak amplitude of the output pulse decrease with the increasing T_g. Moreover, the base width of the output pulse is observed to be T_e-T_g.

In Fig. 2(b) another example is shown. The modulating waveform is not confined within a certain range but has long residual tails as illustrated by curve ① in that figure. The base width of the output pulse cannot be defined. This agrees with the results of Fig. 2(a) in that the peak amplitude of the output pulse decreases with the increase of T_g, but it cannot be concluded whether the half-amplitude duration of the output pulse increases or decreases with increasing T_g.

The above analysis by means of models is simple and easily understood but is not completely exact because the number of partial modulators is not sufficiently large. The case of infinite number of partial modulators can be considered as a type of transmission line with time-varying parameters. Here we will call it "transmission line modulator." The analysis of a transmission line modulator by means of transmission line equations is treated in Appendix I.

Using the general equations developed in Appendix I, the output envelope of the helix-modulated traveling-wave tube pulse generator is calculated in Appendix III. In Appendix III, the steady-state output pattern

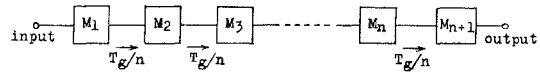

Fig. 1—Equivalent circuit of helix-modulated traveling-wave tube.
M_1, M_2, $\cdots$, M_{n+1}: partial modulators operating with a common time variation and without internal signal delay.
T_g: Signal delay time of traveling-wave tube.
$n+1$: The number of partial modulators (assumed sufficiently large).

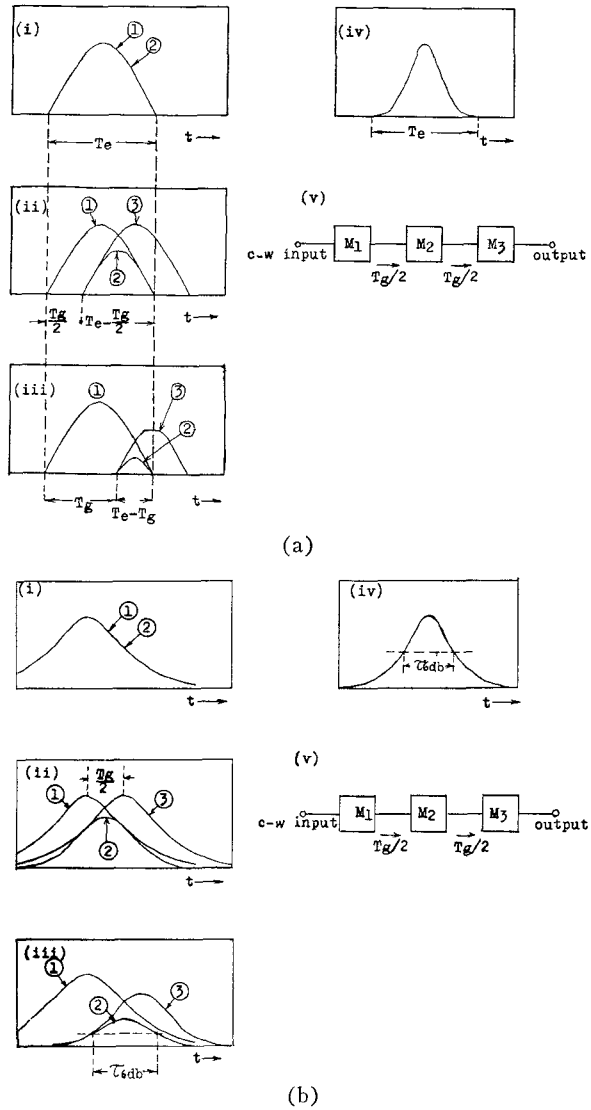

Fig. 2—Example of modulation distortion of transmission line modulator.
(i), (ii), (iii): Waveforms at each partial modulator when $T_g \neq 0$.
①: Modulating waveform of partial modulator.
②: Output waveform of partial modulator.
③: Input waveform of partial modulator.
(iv): Output waveform of transmission line modulator when $T_g=0$ (quasi-static output waveform).
(v): Equivalent circuit of transmission line modulator assumed here.
τ_{6db}: Half-amplitude duration of output pulse.

of the traveling-wave tube has been assumed as a Gaussian function of helix voltage variation.

The results of Appendix III are summarized as follows:

$A(V)$ = Steady-state output of the traveling-wave tube as a function of V.
V = Variation of helix voltage from the synchronous helix voltage.
G = Gain of the traveling-wave tube for $V=0$.
V_{6db} = half-amplitude pattern width of $A(V)$

$$20 \log_{10} A(V) - 20 \log_{10} G = -6\left(\frac{2V}{V_{6db}}\right)^2. \quad (1)$$

τ_{6db} = Half-amplitude duration of output pulse.
v_e = Sweep velocity of helix voltage.
$g_{out(t)}$ = Envelope of output pulse.

$$\tau_{6db} = \frac{V_{6db}}{v_e} \quad (2)$$

$$20 \log_{10} g_{out}(t) - 20 \log_{10} G = -\frac{24}{\tau_{6db}^2}(t - \tfrac{1}{2}T_g)^2 - 2\left(\frac{T_g}{\tau_{6db}}\right)^2. \quad (3)$$

When the helix voltage is modulated with a sinusoidal wave, V is represented as

$$V = \tfrac{1}{2}E \sin(2\pi f_e t), \quad (4)$$

where E is the peak-to-peak value of modulating sinusoidal wave and f_e is the modulating frequency.

If the value of E is sufficiently large (4) is approximated by

$$V = E\pi f_e t \quad (5)$$

for the most part of $g_{out}(t)$. Then we obtain

$$v_e = \frac{dV}{dt} = E\pi f_e \quad (6)$$

$$\tau_{6db} = \frac{V_{6db}}{E\pi f_e}. \quad (7)$$

If the value of E is not sufficiently large, an output pulse of Gaussian envelope will not be obtained as long as the steady-state output pattern of (1) is assumed. In this case it will be considered that the effect of delay time on the output is relatively small and the modulation is quasi-static. Hence, the output pulse duration is obtainable directly from (4),

$$\tau_{6db} = \frac{1}{\pi f_e} \sin^{-1}\left(\frac{V_{6db}}{E}\right). \quad (8)$$

The results described here are all based on (1), and the assumption that the helix-modulated traveling-wave tube is a uniform transmission line modulator operating in a single mode. Those assumptions are realized only approximately in the real traveling-wave tube. Eq. (1) is not valid for helix voltage much different from the synchronous voltage. The traveling-wave tube is not exactly a uniform transmission line modulator because there are certain attenuating regions along the helix. Moreover, the ordinary traveling-wave tube of helix type has three propagating modes: growing wave, attenuating wave, and unattenuating wave. Though the last two modes have negligible contribution to the output when the helix voltage is fixed at the synchronous value, they should not be neglected when the helix voltage is much different from the synchronous value, or when the microwave input to the traveling-wave tube is not sufficiently small, because then their power level becomes comparable to the growing wave level. We will examine in the experiment how many errors are introduced by the approximations used here.

Now we will examine another feature of the helix-modulated traveling-wave tube. It is well known that the carrier frequency of the output pulse shifts from the input carrier frequency [1], [6]. Analysis in Appendix I shows that the delay time of the traveling-wave tube does not cause distortion of phase modulation when the phase constant is swept linearly. Hence, the absolute value of the frequency shift Δf satisfies the following equation:

$$\Delta f = \frac{1}{2\pi} B v_e, \quad (9)$$

where B denotes the phase modulation sensitivity (rad/v), and v_e is given by (6).

Experimental Results

A schematic diagram of the experimental pulse generator is illustrated in Fig. 3. The helix of the traveling-wave tube was modulated with a 40-Mc sinusoidal wave. A part of modulation power was detected to indicate the modulation voltage with the dc meter M_1. The scale of M_1 has been calibrated with the modulation voltage across the parallel tuned circuit. The beam-focusing electrode was modulated optionally at the same frequency in order to separate the output pulse trains with different carrier frequency.

Fig. 4 illustrates the observation of the detected waveforms of the generated pulses by means of the video-sampling oscilloscope. Nominal rise time of the oscilloscope, Lumatron's Model 112-336, was 0.4 nsec.

The detector used here was a 1N26 silicon diode mounted in a specially designed wide-band crystal mount.

Typical frequency characteristics of the detector output for the single frequency microwave input are illustrated in Fig. 5. It will be considered from Fig. 5 that the waveform distortion of the pulse due to the microwave bandwidth of the detector is very small. The stray capacity of the detector measured at the output terminal was about 5 pf. Since the characteristic impedance of the output coaxial cable is 50 ohms, the

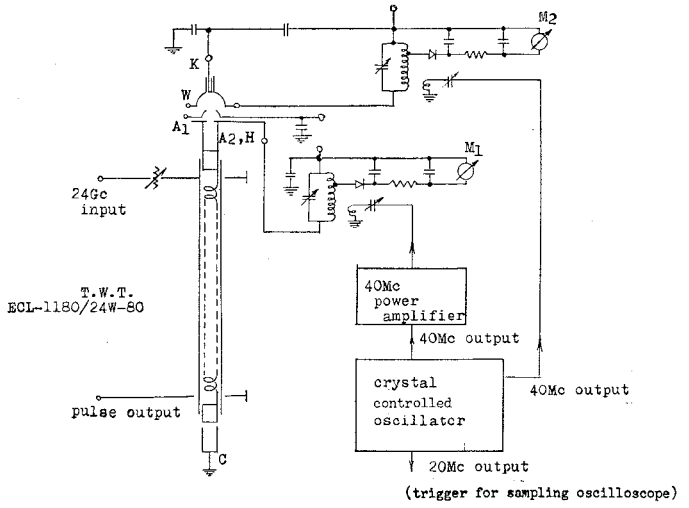

Fig. 3—Experimental circuit of traveling-wave tube pulse generator. dc supply for traveling-wave tube is not illustrated.
M_1: Meter for measuring modulation voltage of helix.
M_2: Meter for measuring modulation voltage of beam-focusing electrode.
K: Cathode.
W: Beam-focusing electrode.
A_1: First anode.
A_2: Second anode.
H: Helix.
C: Collector.

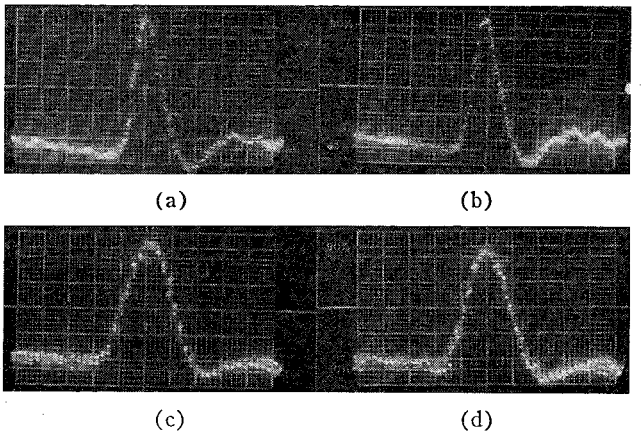

Fig. 4—Observation of generated pulses by means of crystal detector and video-sampling oscilloscope. Photos show generated pulses with lower carrier frequency. Horizontal axis is 1 nsec per major division. (a) $E=740$ v, $P_{in}=2$ mw, $f_{in}=24$ Gc. (b) $E=740$ v, $P_{in}=10$ mw, $f_{in}=24$ Gc. (c) $E=300$ v, $P_{in}=0.5$ mw, $f_{in}=24$ Gc. (d) $E=300$ v, $P_{in}=10$ mw, $f_{in}=24$ Gc.
Horizontal axis: 1 nsec/div.
P_{in}: Microwave input power (mw).
E: Peak to peak value of helix modulating voltage (v).
f_{in}: Input microwave frequency.

time constant of the detector output amounts to 0.25 nsec. But the real time constant is considered smaller than this value because the real stray capacity is the difference of the measured capacity and the equivalent capacity of the short 50-ohm coaxial line which is a part of the crystal mount construction.

The helix-modulated traveling-wave tube generates two kinds of pulses—one has a higher carrier frequency than the input frequency, and the other a lower carrier frequency than the input frequency. Those two kinds of pulses occur alternately. It was observed in this experiment that those two kinds of pulses had identical

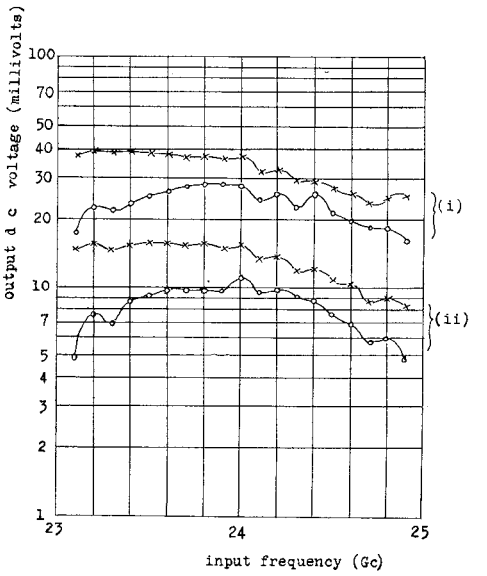

Fig. 5—Frequency characteristics of detector. Marks ○ and × denote measured values for different 1N26-diodes. Load resistance of output terminal was 50 ohms.
(i): Measured value for 3 mw input power.
(ii): Measured value for 1 mw input power.

waveforms and the pulses with lower carrier frequency had larger peak power than the pulses with higher carrier frequency.

Photographs in Fig. 4 show the pulses with lower carrier frequency.

It should be noticed that the waveforms in Fig. 4 are almost independent of the microwave input power. When the traveling-wave tube used here operates with the synchronous helix voltage as a normal amplifier, its output power saturates at a microwave input power as low as 1 or 2 mw. It is noticed that the large signal operation of the traveling-wave tube hardly deteriorates the output waveforms of the pulse generator.

Fig. 6 illustrates the experimental results obtained by means of waveguide interferometer. Construction of the waveguide interferometer used in this experiment is sketched in Fig. 24. The variable delay line consists of a circular waveguide operating with TE_{01} mode, non-contacting short plunger, and TE_{01} mode excitor. The short plunger runs with a constant speed automatically in the circular waveguide. The detector used here is of the same type as one used together with the sampling oscilloscope. The detector output is loaded with a capacitor of 1000 pf. If we assume the output circuit resistance is 100 ohms, the time constant of the detector output becomes 0.1 μsec. In this experiment, the generated pulses with higher carrier frequency were suppressed by applying a 40-Mc sinusoidal wave to the beam-focusing electrode of the traveling-wave tube, and only the generated pulses with lower carrier frequency were observed. Hence, the repetition cycle of the output pulses was 25 nsec and much smaller than the time constant of the detector output. Hence it will be concluded that the detector operates as a peak detector, and the output patterns of the interferometer

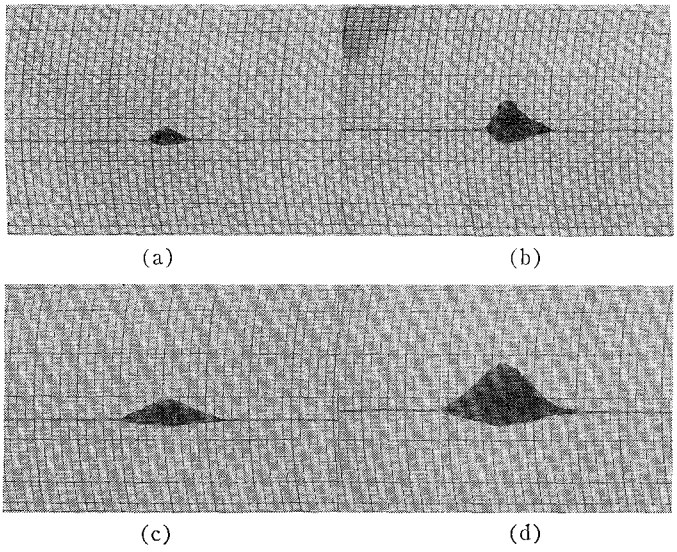

(a) (b)

(c) (d)

Fig. 6—Interferometer patterns of generated pulses. Pulses with lower carrier frequency are illustrated. (a) $E=740$ v, $P_{in}=5$ mw, $f_{in}=24$ Gc. Horizontal axis: 1.75 nsec per major division. (b) $E=740$ v, $P_{in}=10$ mw, $f_{in}=24$ Gc. Horizontal axis: 1.75 nsec per major division. (c) $E=300$ v, $P_{in}=0.5$ mw, $f_{in}=24$ Gc. Horizontal axis: 1.75 nsec per major division. (d) $E=300$ v, $P_{in}=2$ mw, $f_{in}=24$ Gc. Horizontal axis: 1.75 nsec per major division.
P_{in}: Microwave input power of traveling-wave tube (mw).
E: Peak to peak value of helix modulating voltage (v).
f_{in}: Input microwave frequency.

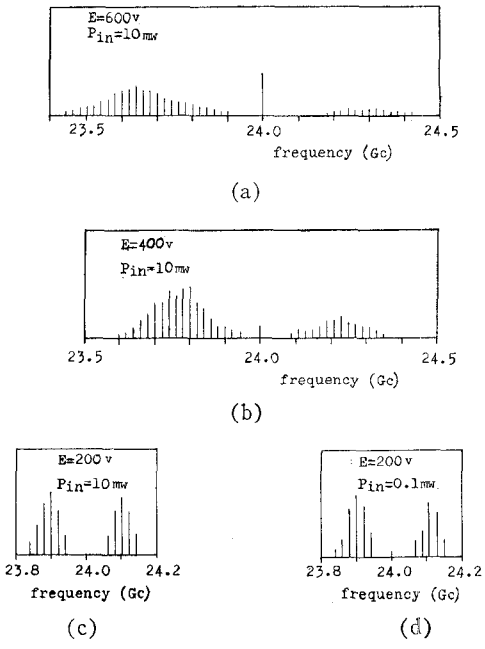

Fig. 7—Power spectra of generated pulses.
P_{in}: Microwave input of traveling-wave tube (mw).
E: Peak to peak value of helix modulating voltage (v).
Input microwave frequency is 24.0 Gc.

can be used to obtain half-amplitude duration of the pulses (see Appendix IV).

Fig. 7 illustrates measured power spectra of the generated pulses. In this experiment we used a variable filter and a crystal detector. The variable filter is a cylindrical cavity with a movable short plunger at one end. Its parameters at 24 Gc are:

loaded $Q=760$
unloaded $Q=2500$
insertion loss $=1.7$ db
half-amplitude bandwidth $=31.6$ Mc.

The fine structures of the spectra were not observed exactly because the bandwidth of the variable filter was not sufficiently narrow in comparison with the separation of the spectral components. It was most satisfactory for observing the major features of the spectra. The output of the variable filter was rectified with a quadratic detector and measured with a dc meter. It is observed from Fig. 7(a) and (b) that the pulses with higher carrier frequency have lower power than those with lower carrier frequency, and from Fig. 7(c) and (d) that the pulse width is almost independent of the microwave input power of the traveling-wave tube. Those results agree with the observation using the sampling oscilloscope. It should be noticed that there are spectral components having the identical frequency with the input frequency of 24 Gc in Fig. 7(a) and (b). Those components are considered to be caused by certain propagating modes having phase velocity almost independent of the helix voltage.

Now we will obtain the half-amplitude duration of the generated pulses from the above-mentioned results in order to compare the experimental results with the theory.

The half-amplitude width of the static output pattern of the traveling-wave tube used here was about 100 v. Hence, we obtain the theoretical value of τ_{6db} from (7) or (8):

$$\tau_{6db} = 7.96 \sin^{-1}\left(\frac{100}{E}\right) \text{(nsec)}, \tag{10}$$

because we have set

$$V_{6db} = 100 \text{ v}$$
$$f_e = 40 \text{ Mc}.$$

Eq. (10) is calculated in Fig. 8. The symbol E denotes the peak to peak value of the helix modulating voltage in volts.

Since the waveforms in Fig. 4 represent the power waveforms of the original carrier pulses, their quarter-amplitude width equals the half-amplitude duration of the original carrier pulses. Fig. 9 illustrates the half-amplitude duration of the generated pulses thus obtained.

Fig. 10 illustrates the half-amplitude duration of the generated pulses obtained from the interferometer patterns in Fig. 6. In the course of obtaining it, we have assumed that the envelope of the pulse is Gaussian and made use of D_t as illustrated in Fig. 26.

Fig. 11 illustrates the half-amplitude duration of generated pulses obtained from the power spectrum in Fig. 7. Here we have assumed that the envelope of the pulse is Gaussian and made use of the following relation:

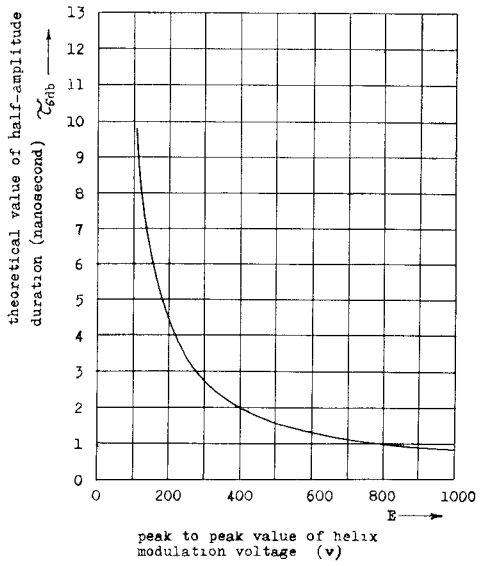

Fig. 8—Half-amplitude pulse duration vs helix modulating voltage [theoretical calculation from (10)].

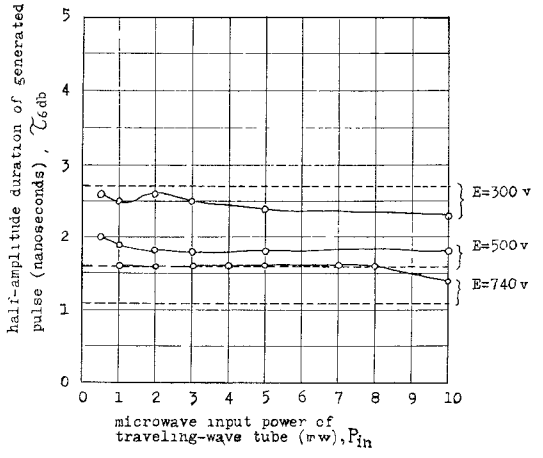

Fig. 9—Half-amplitude duration of generated pulses measured with wide-band detector and video-sampling oscilloscope.
Mark ○ denotes experimental value.
E: Peak to peak value of helix modulation voltage.
Dotted lines denote calculations for $V_{6db}=100$ v.

$$W_{3db}\cdot\tau_{6db} = 0.63, \tag{11}$$

where W_{3db} is the half-power width of the spectrum and τ_{6db} is the half-amplitude duration of the pulse.

The pulse durations obtained from the above-mentioned three methods do not necessarily coincide with each other nor with the calculations. The results in Fig. 9 suggest that the observation apparatus composed of the detector and the video-sampling oscilloscope has a considerable amount of rise time because the measured pulse duration becomes larger than the calculated value when it becomes small. The measured pulse duration in Fig. 10 varies as a function of the input power of the traveling-wave tube. Analysis has not been performed as to whether this variation originates from the characteristics of the generated pulses or from the errors in the experimental apparatus. The interferometer pattern should be symmetrical if the interferometer operates

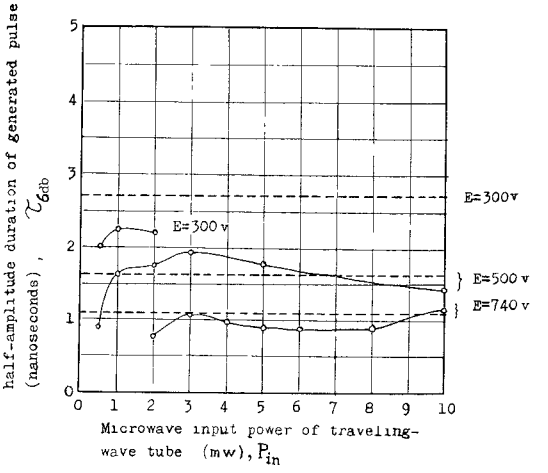

Fig. 10—Half-amplitude duration of generated pulses measured with interferometer.
Mark ○ denotes experimental value.
Dotted lines denote calculations for $V_{6db}=100$ v.

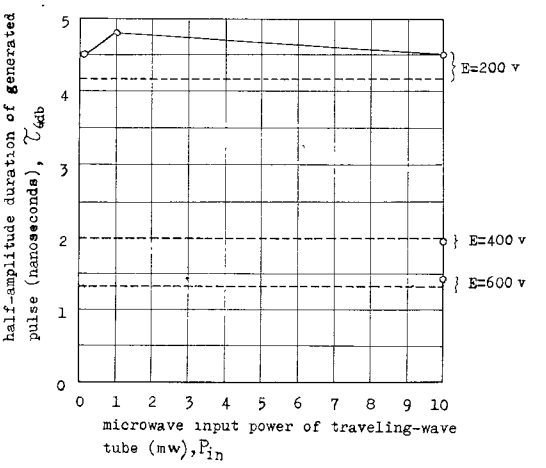

Fig. 11—Half-amplitude duration of generated pulses obtained from power spectrum (pulse envelope is assumed Gaussian).
Dotted lines are calculations for $V_{6db}=100$ v.
E: Peak to peak value of helix modulating voltage.
Mark ○ denotes experimental value.

properly, but the measured patterns are considerably unsymmetrical when the modulating voltage is large. This situation suggests that waveform distortion is present in the variable delay line of the interferometer. The measured duration of the generated pulses coincides well with the calculation in spite of the measured unsymmetrical pattern. The power spectrum measurement could be performed only for the pulses with comparatively large power of the spectral components. Hence, the generated pulses could not be observed with this method when the helix modulating voltage was large and the microwave input power of the traveling-wave tube was small.

The measured pulse duration in Fig. 11 shows a good agreement with the calculation. This result suggests that the envelope of the generated pulses is approximately Gaussian.

Fig. 12 illustrates the carrier frequency shift of the generated pulses. The experimental values have been

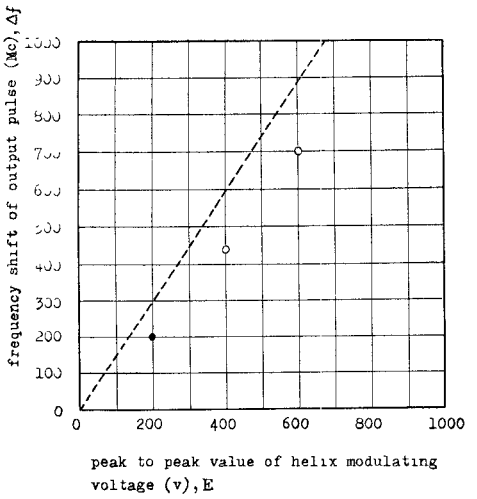

Fig. 12—Carrier frequency shift of output pulse from input frequency.
○: Measured value when microwave input power is 10 mw.
●: Measured value when microwave input power is 0.1, 1, or 10 mw.
Dotted line is calculated value.
Input microwave frequency is 24 Gc.

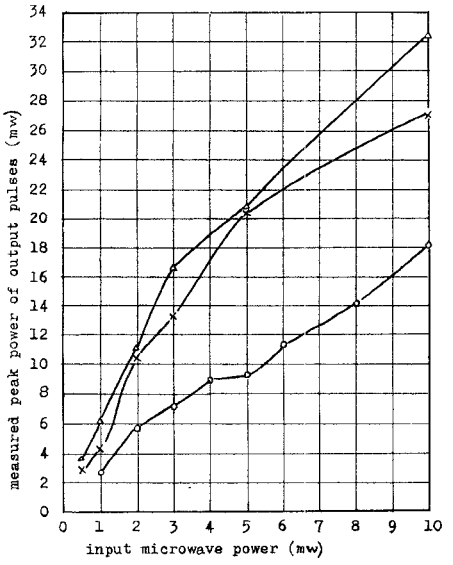

Fig. 13—Example of measured peak power of generated pulses.
○: $E=740$ v.
×: $E=500$ v.
△: $E=300$ v.
E is peak to peak value of helix modulating voltage (v).

derived from Fig. 7. The theoretical curve has been calculated from (6) and (9) assuming

$$B = 0.0735 \text{ rad/v}$$

$$f_e = 40 \text{ Mc.}$$

The value of B assumed here has been obtained from the static measurement of the traveling-wave tube.

The peak power of the generated pulse will be interesting for application. An example of experimental results is illustrated in Fig. 13. In this measurement we used the measuring device composed of the wide-band crystal detector and the video-sampling oscilloscope. The vertical axis of the oscilloscope has been calibrated with respect to the peak power of the input pulse having such a long duration that the waveform distortion was negligible. The results in Fig. 13 contain errors because of the restricted frequency bandwidth of the measuring device. In this experiment the microwave frequency band of the detector was fairly broad, and the over-all bandwidth of the measuring device was determined mainly by the video part of the circuit. Hence, the observed height of pulses in Fig. 13 represents the correct peak power of the pulses when their rise time is large, but represents the mixture of the peak and average power of the pulses when their rise time is small.

Effects of Helix Delay Time on Generated Pulses

It was already mentioned that the helix delay time of the traveling-wave tube influences the duration, the shape and the power of the generated pulses. Theoretical analysis and approximate calculations in Appendixes I and III show that the power of the generated pulses is influenced most seriously with the helix delay time when we assume that the steady-state output of the traveling-wave tube is a Gaussian function of the helix voltage. The peak and average power of the generated pulses are calculated as a function of τ_{6db}/T_g in Appendix III, where τ_{6db} and T_g are half-amplitude duration of the generated pulses and helix delay time of the traveling-wave tube, respectively. When we cannot measure τ_{6db} directly, it will be convenient to rewrite τ_{6db}/T_g as

$$\frac{\tau_{6db}}{T_g} = \frac{1}{\pi f_e T_g} \sin^{-1}\left(\frac{V_{6db}}{E}\right) \fallingdotseq \frac{1}{\pi f_e T_g} \frac{V_{6db}}{E} \qquad (12)$$

referring to (7) or (8).

In the case that the influence of the helix delay time is not present, the peak power of the generated pulses is independent of the helix modulating voltage and the average power is approximately proportional to the reciprocal of the helix modulating voltage.

Fig. 14 shows the variation of peak and average power of the generated pulses as a function of the reciprocal of helix modulating voltage when the helix delay time is present or absent. Curves A and C denote the peak and average power of the generated pulses when the helix delay time is zero. Curves B and D denote the peak and average power of the generated pulses when the helix delay time is not zero. Exact calculations for the curve B and D are presented in Appendix III. The curve B or D is largely different from the curve A or C. Hence, we will be able to verify the influence of the helix delay time by measuring the peak or average power of the generated pulses as a function of the reciprocal of helix modulating voltage.

Fig. 15 shows the experimental result. The vertical axis denotes the peak amplitude of the detected pulses observed on the screen of the video-sampling oscilloscope.

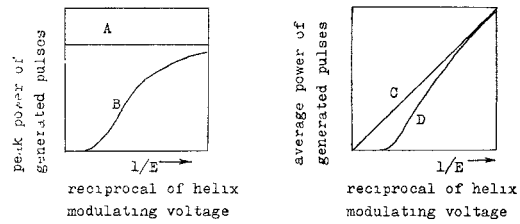

Fig. 14—Variation of peak and average power of generated pulses as a function of reciprocal of helix modulating voltage when helix delay time is present or absent. Curves A and C denote peak and average power when helix delay time is absent. Curves B and D denote peak and average power when helix delay time is present.

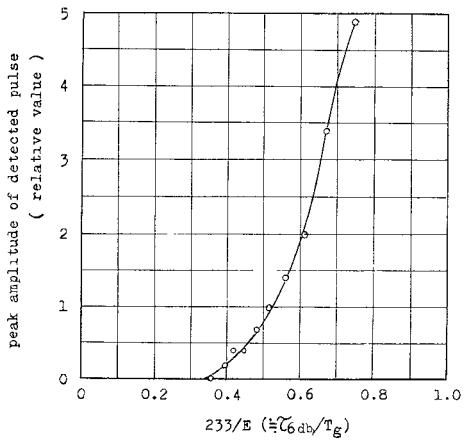

Fig. 15—Observation of power level of generated pulse.
E is peak to peak value of helix modulating voltage.
Microwave input power: 0.1 mw.
Microwave input frequency: 24 Gc.

Since the wide-band detector used here is quadratic, the vertical axis is proportional to the peak power of the original carrier pulse on the assumption that the frequency bandwidth of the detector and the video-sampling oscilloscope is sufficiently wide.

But this assumption is not valid exactly. The frequency characteristic of this device is restricted mainly by the stray capacity of the detector output circuit and rise time of the sampling oscilloscope. Hence, the vertical axis represents a mixture of the peak and average power of the original carrier pulses.

The horizontal axis denotes τ_{6db}/T_g, because in this experiment

$f_e = 40$ Mc
$T_g = 3.42$ nsec
$V_{6db} = 100$ v

$$\frac{\tau_{6db}}{T_g} \fallingdotseq \frac{V_{6db}}{\pi f_e T_g} \cdot \frac{1}{E} = 233 \frac{1}{E} \cdot \tag{13}$$

The result in Fig. 15 is different from the curves A or C in Fig. 14 but shows a good agreement with the curves B or D in Fig. 14 or the calculated curves in Fig. (22) or (23).

Traveling-Wave Tube

The traveling-wave tube used in this experiment is the ECL-1180/24W80 [8]. It is a helix-type traveling-wave tube having a comparatively small gain and power output. It was the only available tube in the 24-Gc region when we performed this experiment. But as the new tube ECL-1207/24W90 with large gain and power output was developed lately, it will be convenient to use it in the future.

The standard characteristics of the tube ECL-1180/24W80 are as follows:

Operating frequency (center)	24 Gc.
First anode voltage	500∼700 v.
Beam-focusing electrode voltage	0∼−50 v.
Collector current	2 ma.
Synchronous helix voltage (small signal input)	2000±100 v.
Small signal gain	15 db or more.
Saturation output	20 mw or more.
Helix length	80 mm.

We have measured the characteristics of the tube used in this experiment.

Frequency dependence of small signal gain for fixed helix voltage is shown in Fig. 16. The half-power frequency bandwidth is about 3 Gc. This measurement was performed by means of the oscillation method because the wide-band signal generator was not available. Hence, it is considered that the result contains some errors due to the frequency characteristics of the insertion loss of the variable filter in the oscillation loop.

The phase modulation sensitivity of the traveling-wave tube was measured with the bridge circuit. The measured value was 0.0735 rad/v.

Examples of the static output patterns are shown in Fig. 17. The vertical axis of the figure represents the relative output power. The output amplitude pattern $A(V)$ used in the calculation corresponds to the square root of the vertical axis. We observe that side patterns are present for large input power. These side patterns result from the interference between the growing wave and the attenuating or unattenuating wave in the traveling-wave tube.

The helix delay time of the traveling-wave tube was obtained from the measurement of the frequency-phase relation of the traveling-wave tube. The bridge circuit used for the experiment is sketched in Fig. 18. The traveling-wave tube and a variable attenuator are inserted in the arm 1. A calibrated phase shifter is inserted in the arm 2. Balancing condition of the bridge is as follows:

$$\beta l_2 + \Theta = \beta l_1 + \theta + 2\pi n \tag{14}$$

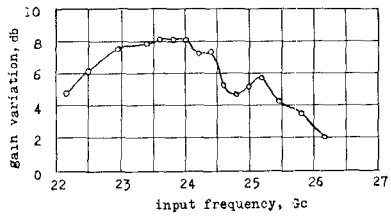

Fig. 16—Frequency characteristics of small signal gain for fixed helix voltage.
Helix voltage: 1800 v.
Collector current: 1.4 ma.

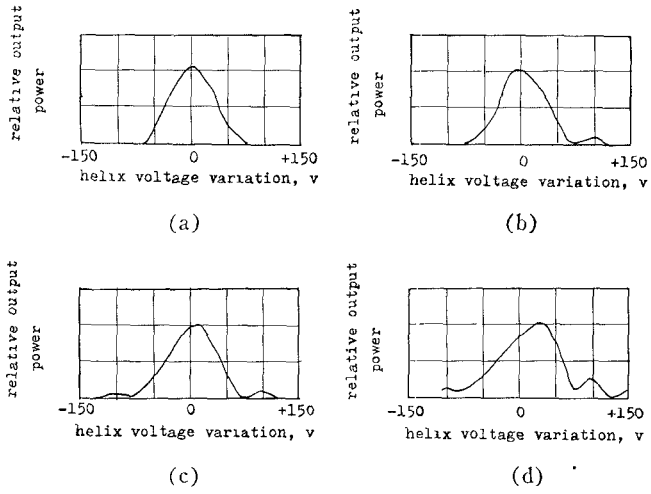

Fig. 17—Static output pattern of used traveling-wave tube. Input microwave frequency: 24 Gc.

	Input Power	Collector Current
(a)	0.1 mw	1.4 ma
(b)	0.1 mw	1.0 ma
(c)	1.0 mw	1.0 ma
(d)	8.0 mw	1.0 ma

where

β = phase constant of waveguide
l_1 = total length of waveguide in arm 1
l_2 = total length of waveguide in arm 2
Θ = phase shift of calibrated phase shifter
θ = phase shift of traveling-wave tube
n = integer.

Differentiating (14) with respect to the angular frequency ω we obtain

$$\frac{\partial(\beta l_2)}{\partial\omega} + \frac{\partial\Theta}{\partial\omega} = \frac{\partial(\beta l_1)}{\partial\omega} + \frac{\partial\theta}{\partial\omega} \tag{15}$$

or

$$T_g = \frac{\partial\theta}{\partial\omega} = \frac{\partial\Theta}{\partial\omega} + \tau(l_2 - l_1) \tag{16}$$

where T_g is the helix delay time and τ is the delay time of the waveguide per unit length. In the course of derivation of (16), we assumed that the delay time of the attenuator and the phase shifter is approximately equal

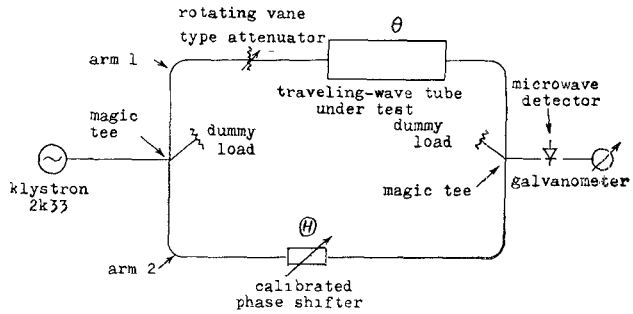

Fig. 18—Bridge circuit for measuring delay time of traveling-wave tube.
θ: Phase shift of traveling-wave tube.
Θ: Phase shift of calibrated phase shifter.

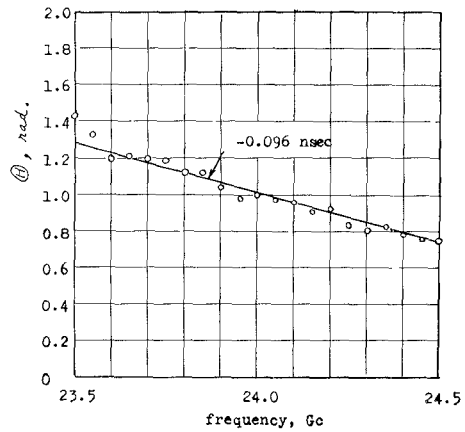

Fig. 19—Measurement of traveling-wave tube delay time.
Θ: Phase shift of calibrated phase shifter when bridge circuit of Fig. 18 is balanced.
Helix voltage: 1800 v.

to the delay time of waveguide having the same length. Therefore the length l_1 and l_2 include the length of the attenuator and phase shifter.

The experimental value of Θ is illustrated in Fig. 19 as a function of the frequency. The straight solid line in the figure corresponds to -0.096 nsec. The small ripples of the experimental value is considered to be caused by weak echo in the circuit. The value of $l_2 - l_1$ and τ was as follows:

$$l_2 - l_1 = 0.859 \text{ meter}$$
$$\tau = 4.10 \text{ nsec/m}.$$

Therefore we obtain

$$T_g = 3.42 \text{ nsec}.$$

Conclusions

A nanosecond carrier pulse generator using a helix-modulated traveling-wave tube in the 24-Gc region was investigated experimentally and theoretically. It was discovered that the helix delay time of the traveling-wave tube has a large effect on the characteristics of the output pulses. In particular, its effect on the peak power of output pulses is very large.

It was found from the theoretical analysis that the peak power of output pulses decreases rapidly with decreasing τ_{6db}/T_g when τ_{6db}/T_g is smaller than unity, where τ_{6db} and T_g are half-amplitude duration of output pulses and helix delay time of the traveling-wave tube, respectively.

This phenomenon was verified also in the experiment.

To remove this defect, the following methods may be considered:

1) Constructing a traveling-wave tube with small helix delay time.
2) Operating the traveling-wave tube with large microwave input.
3) Modulating the traveling-wave tube helix with a traveling-wave voltage instead of standing-wave voltage.

Method 1) is the most straightforward, but it will be necessary to design a special traveling-wave tube. Method 2) can be applied easily, but there arises a possibility that the pulse waveform is distorted due to the nonlinear operation of the traveling-wave tube. Method 3) requires reconstruction of the tube. In the last case, it will be convenient to use the helix as a part of a traveling-wave resonator in order to reduce modulating power.

The output pulses were observed with three kinds of apparatus: video-sampling oscilloscope with microwave detector, interferometer, and spectrum analyzer. Pulse widths measured with these apparatus agreed well with each other and with theoretical calculations with the exception of partial error. The pulse waveform was not observed accurately when the pulse width was as short as 1 nsec. It will be necessary to improve the sampling oscilloscope and the microwave detector and to reduce their rise time in order to observe accurately the waveform of the pulses.

Appendix I

Theoretical Analysis of Transmission Line Modulator

We will consider a transmission line with variable transmission constant $\gamma(t, z)$. Where t and z are time and distance along the transmission line, respectively.

$$\gamma(t, z) = \alpha(t, z) + j\beta(t, z). \tag{17}$$

We will assume that $\alpha(t, z)$ and $(\partial/\partial\omega)\ \beta\ (t, z)$ have negligibly small frequency dependence in the frequency region considered, where ω is angular frequency.

If signal distortion due to echo and mode conversion is not present, the signal propagates along the transmission line with constant group velocity and is affected only by $\gamma\ (t, z)$.

The signal waveform is assumed as

$$g(t, z) \exp [j\omega_0 t + j\theta(t, z)],$$

where $g(t, z)$ is the envelope, $\theta(t, z)$ is the phase factor, and ω_0 is the angular frequency of carrier.

Then the envelope $g(t, z)$ and angular frequency modulation

$$\Omega(t, z) = \frac{\partial}{\partial t}\theta(t, z)$$

satisfy the following equations:

$$g(t - \tau_g dz, z) \exp [-\alpha(t, z)dz] = g(t, z + dz) \tag{18}$$

$$\Omega(t - \tau_g dz, z) - \frac{\partial}{\partial t}\beta(t, z)dz = \Omega(t, z + dz), \tag{19}$$

where τ_g is signal delay time per unit length of the transmission line.

From these equations the following transmission line equations are derived:

$$\tau_g \frac{\partial g}{\partial t} + \frac{\partial g}{\partial z} + \alpha g = 0 \tag{20}$$

$$\tau_g \frac{\partial \Omega}{\partial t} + \frac{\partial \Omega}{\partial z} + \frac{\partial \beta}{\partial t} = 0. \tag{21}$$

These equations are Lagrange's linear equations. The solutions are easily obtained as

$$g(t, z) = \exp [F_1(t - \tau_g z)] \cdot \exp\left[-\int_0^z \alpha(\tau_g\xi + t - \tau_g z, \xi)d\xi\right] \tag{22}$$

$$\Omega(t, z) = F_2(t - \tau_g z) - \int_0^z \frac{\partial}{\partial t}\beta(\tau_g\xi + t - \tau_g z, \xi)d\xi, \tag{23}$$

where $F_1(\ )$ and $F_2(\ )$ are arbitrary functions which are derived from boundary conditions.

Replacing $F_1(t)$ and $F_2(t)$ with $g(t, 0)$ and $\Omega(t, 0)$ respectively, we obtain

$$g(t, z) = g(t - \tau_g z, 0) \cdot \exp\left[-\int_0^z \alpha(\tau_g\xi + t - \tau_g z, \xi)d\xi\right] \tag{24}$$

$$\Omega(t, z) = \Omega(t - \tau_g z, 0) - \int_0^z \frac{\partial}{\partial t}\beta(\tau_g\xi + t - \tau_g z, \xi)d\xi. \tag{25}$$

Moreover, we obtain

$$g_{out}(t) = g_{in}(t - \tau_g L) \cdot \exp\left[-\int_0^L \alpha(\tau_g\xi + t - \tau_g L, \xi)d\xi\right] \tag{26}$$

$$\Omega_{out}(t) = \Omega_{in}(t - \tau_g L) - \int_0^L \frac{\partial}{\partial t}\beta(\tau_g\xi + t - \tau_g L, \xi)d\xi \tag{27}$$

for the transmission line modulator with length of L, where

$g_{in}(t)$ = envelope of input signal
$g_{out}(t)$ = envelope of output signal
$\Omega_{in}(t)$ = angular frequency modulation of input signal
$\Omega_{out}(t)$ = angular frequency modulation of output signal.

We will discuss some typical cases of (26) and (27) to examine the performance of the transmission line modulator.

Amplitude Modulator of Standing-Wave Type

We will examine a case in which the modulating voltage V is applied as a standing wave along the transmission line. $\alpha(t, z)$ is rewritten as

$$\alpha(t, z) = u_0(z) + u(z)v(V). \tag{28}$$

Static performance of the modulator is represented as a function of the static modulating voltage V:

$$g_{out} = G \cdot g_{in} \cdot \exp\left[-Mv(V)\right] \tag{29}$$

where

$$G = \exp\left[-\int_0^L u_0(\xi)d\xi\right] \tag{30}$$

$$M = \int_0^L u(\xi)d\xi. \tag{31}$$

When V is a function of t, we set

$$V = V(t) \tag{32}$$

and substitute (28) into (26):

$$g_{out}(t) = G \cdot g_{in}(t - \tau_g L) \cdot \exp\left[-\int_0^L u(\xi)v\{V(\tau_g\xi + t - \tau_g L)\}d\xi\right]. \tag{33}$$

It will be advantageous to rewrite (33) by the static performance function in order to discuss the difference between real and static characteristics of the modulator. The static performance function $A(V)$ is defined as

$$A(V) = G \exp\left[-Mv(V)\right]. \tag{34}$$

Then (33) is rewritten as

$$g_{out}(t) = g_{in}(t - \tau_g L) \cdot \exp\left[\frac{1}{M}\int_0^L u(\xi) \ln A\{V(\tau_g\xi + t - \tau_g L)\}d\xi\right], \tag{35}$$

where the symbol ln denotes the natural logarithmic function. Or, if we set

$$A[V(t)] = f(t) \tag{36}$$

(35) is rewritten as

$$g_{out}(t) = g_{in}(t - \tau_g L) \cdot \exp\left[\frac{1}{M}\int_0^L u(\xi) \ln f(\tau_g\xi + t - \tau_g L)d\xi\right] \tag{37}$$

and $f(t)$ is a hypothetical modulation function derived from the static characteristic of the modulator.

Eq. (37) is made simple in the case of constant $u(\xi)$ as follows:

$$g_{out}(t) = g_{in}(t - \tau_g L) \cdot \exp\left[\frac{1}{L}\int_0^L \ln f(\tau_g\xi + t - \tau_g L)d\xi\right] = g_{in}(t - T_g) \exp\left[\frac{1}{T_g}\int_0^{T_g} \ln f(t - x)dx\right] \tag{38}$$

where

$$T_g = \tau_g L. \tag{39}$$

If T_g is sufficiently small, the second factor of the right-hand side of (38) is approximated as

$$\exp\left[\frac{1}{T_g}\int_0^{T_g} \ln f(t - x)dx\right] \fallingdotseq f(t) - \tfrac{1}{2}T_g f'(t). \tag{40}$$

As a result it is concluded that the modulation distortion of a transmission line modulator is proportional to the delay time of the transmission line and the time derivative of the modulation function when the distribution of modulation along the transmission line is uniform and the distortion is small.

Eq. (37) or (38) can be utilized to investigate the performance of the helix-gated traveling-wave tube pulse generator. Calculations of its output pulse shape is performed in Appendix III.

Eq. (40) is applied to examine how many errors are present when the output pattern of a traveling-wave tube is measured as a function of swept helix voltage.

Amplitude Modulator of Traveling-Wave Type

An amplitude modulator in which the modulating voltage is applied to the transmission line as a traveling wave will be examined here. For simplicity, modulation sensitivity is assumed to be uniform along the modulator. Then $\alpha(t, z)$ may be represented as

$$\alpha(t, z) = \alpha(V) \tag{41}$$

$$V = V(t - \tau_M z) \tag{42}$$

where τ_M denotes the propagation time of the modulating voltage V per unit length of the modulator.

Static and dynamic characteristics are given as

$$g_{out} = g_{in} \cdot \exp\left[-L\alpha(V)\right] \tag{43}$$

$$g_{out}(t) = g_{in}(t - \tau_g L) \cdot \exp\left[-\int_0^L \alpha\{V(\tau_g\xi + t - \tau_g L - \tau_M\xi)\}d\xi\right]. \tag{44}$$

Then, the dynamic performance equation (44) can be represented in terms of static characteristic:

$$g_{out}(t) = g_{in}(t - T_g) \cdot \exp\left[-\frac{1}{L}\int_0^L \ln A\{V(\tau_g\xi + t - \tau_g L - \tau_M\xi)\}d\xi\right] = g_{in}(t - T_g) \cdot \exp\left[\frac{-1}{T_g - T_M}\int_{T_g}^{T_M} \ln A\{V(t - x)\}dx\right], \tag{45}$$

where

$$A(V) = \exp\left[-L\alpha(V)\right] \tag{46}$$

$$T_g = \tau_g L, \qquad T_M = \tau_M L. \tag{47}$$

It is easily seen that modulation distortion is approximately proportional to $(T_g - T_M)$ and $(d/dt)A\{V(t)\}$ for a sufficiently small $(T_g - T_M)$.

Eq. (45) may be applied to the traveling-wave tube modulated with beam forming electrode. A density-modulated electron beam flows with almost the same velocity as the microwave signal propagating on the coupled transmission line of circuit and electron beam. The value of $(T_g - T_M)$ is considered very small. As a result, modulation distortion due to the transmission line modulation is very small.

Frequency or Phase Modulator [6]

In the case of the frequency or phase modulator, almost the same treatment is available as in the case of the amplitude modulator.

A traveling-wave tube with helix modulation operates not only as an amplitude modulator but also as a phase modulator of standing-wave type. The analysis can be performed with (27).

Here, we will calculate the carrier frequency shift of the output pulse of the helix-modulated traveling-wave tube pulse generator.

In this case it may be assumed that the helix voltage is swept linearly in the output pulse duration and that the variable part of the phase constant is almost linearly dependent on the helix voltage variation. That is, the variable part of the phase constant $\beta(t, z)$ satisfies the following equation:

$$\beta(t, z) = u(z)v_e t, \tag{48}$$

where v_e denotes the sweep velocity of helix voltage. Substituting into (27) we obtain

$$\Omega_{\text{out}}(t) - \Omega_{\text{in}}(t - \tau_g L) = -Bv_e \tag{49}$$

$$B = \int_0^L u(\xi)d\xi. \tag{50}$$

The parameter B is the static-phase modulation sensitivity of the traveling-wave tube.

Then the carrier frequency shift of the output pulse with reference to input carrier frequency is represented as

$$\Delta f = \frac{1}{2\pi} Bv_e. \tag{51}$$

It must be noticed that the present result is independent of the delay time T_g.

Appendix II

Characteristics of Generated Pulse—Case 1

Here we will treat a somewhat idealized case in which the steady-state output of the traveling-wave tube is confined within a specified range of helix voltage and vanishes outside.

The function $f(t)$, defined by (36), is also confined in a specified range of time, say T_e, because $A(V)$ is confined in a specified range of voltage and V is swept linearly.

If we assume the input signal is a continuous wave of unit amplitude, the output envelope is represented as

$$g_{\text{out}}(t) = \exp\left[\frac{1}{M}\int_0^L u(\xi)\ln f(\tau_g\xi + t - \tau_g L)d\xi\right] \tag{52}$$

from (37).

We will calculate the base pulse width of $g_{\text{out}}(t)$ from (52) (see Fig. 20). $f(t)$ satisfies the following equations:

$$\begin{aligned} f(t) &> 0; \qquad |t| < \tfrac{1}{2}T_e \\ f(t) &= 0; \qquad |t| > \tfrac{1}{2}T_e. \end{aligned} \tag{53}$$

Then, $f(\tau_g\xi + t - \tau_g L)$ has nonzero value in the domain I, and vanishes in the domain II and III as indicated in Fig. 21,

$$\left.\begin{aligned} &\text{domain I; } |\tau_g\xi + t - \tau_g L| < \tfrac{1}{2}T_e \\ &\text{domain II; } \tau_g\xi + t - \tau_g L > \tfrac{1}{2}T_e \\ &\text{domain III; } \tau_g\xi + t - \tau_g L < -\tfrac{1}{2}T_e \end{aligned}\right\}. \tag{54}$$

The integration path of (52) is on a straight line parallel to the ξ axis and from $\xi = 0$ to $\xi = L$, where $T_g = \tau_g L$.

It is easily seen, the nonzero value of $g_{\text{out}}(t)$ is obtained only if $f(\tau_g\xi + t - \tau_g L)$ does not vanish for all values of ξ along the integration path. This condition for obtaining the nonzero value of $g_{\text{out}}(t)$ is satisfied with t

$$\text{from} \quad -\left(\frac{T_e}{2} - T_g\right) \quad \text{to} \quad \frac{T_e}{2}.$$

Therefore, $g_{\text{out}}(t)$ has nonzero value in a duration of

$$\tau = \frac{T_e}{2} + \left(\frac{T_e}{2} - T_g\right) = T_e - T_g. \tag{55}$$

Obviously τ denotes the base width of the output pulse.

It is remarkable that the base width of the output pulse is the difference of the helix gating duration T_e and helix delay time T_g. If we could obtain a traveling-wave tube whose steady-state output completely vanishes outside of a specified range of the helix voltage, very short pulse would be generated by means of the helix gating method because the pulse width is reduced by the helix delay time.

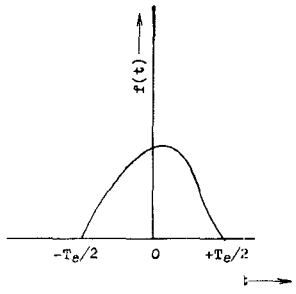

Fig. 20—Example of $f(t)$.

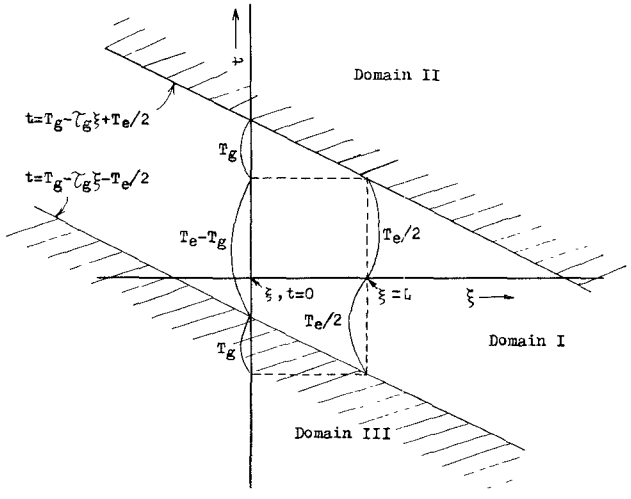

Fig. 21—Three domains in which $f(\tau_g\xi+t-\tau_g L)$ has nonzero value or vanishes.

Appendix III

Characteristics of Generated Pulse—Case 2

It can hardly be assumed that the steady-state output of the real traveling-wave tube completely vanishes outside of a certain range of helix voltage.

According to Pierce's calculation [7] the growing wave parameter x_1 is a function of the velocity parameter b of the electron beam, and its curve is similar to the upper half of an ellipsoid when the effect of the space charge is present. Therefore, it will be reasonable to take the following output amplitude pattern $A(V)$ as a function of helix voltage variation V for the purpose of calculating the output pulse shape.

$$\left.\begin{aligned} A(V) &= G\exp\left[k\sqrt{1-(2V/V_0)^2}-k\right]; && (2V/V_0)^2 \le 1, \\ &= G\exp(-k); && (2V/V_0)^2 \ge 1 \end{aligned}\right\}. \tag{56}$$

Eq. (56) is approximated with

$$A(V) = G\exp\left[-\frac{k}{2}\left(\frac{2V}{V_0}\right)^2\right] \tag{57}$$

for small absolute value of V/V_0.

Here, we will use (57) for the calculation. Calculation with (57) is not exact, but is a fairly good approximation for the most part of $A(V)$ when G and k are sufficiently large. Moreover (57) makes the calculation very simple.

Assuming the traveling-wave tube pulse generator as a uniform transmission line modulator with the linear swept modulating voltage, we obtain the following equations by referring to Appendix I:

$$f(t) = A(v_e t) = G\exp\left[-\frac{k}{2}\left(\frac{2v_e t}{V_0}\right)^2\right] \tag{58}$$

$$= G\exp\left[-\frac{k}{2}\left(\frac{2t}{T_e}\right)^2\right]$$

$$g_{\text{out}}(t) = \exp\left[\frac{1}{T_g}\int_0^{T_g}\ln f(t-x)dx\right] \tag{59}$$

$$T_e = V_0/v_e \tag{60}$$

where $g_{\text{in}}(t)$ is assumed a continuous wave of unit amplitude, and v_e denotes the sweep velocity of the helix voltage.

Substituting (58) into (59) we obtain

$$20\log_{10}[g_{\text{out}}(t)] - 20\log_{10}G = -\frac{2A}{T_e^2}(t-\tfrac{1}{2}T_g)^2 - \frac{A}{6}\left(\frac{T_g}{T_e}\right)^2 \tag{61}$$

where

$$A = 8\cdot 686k. \tag{62}$$

Therefore, the half-amplitude pulse duration $\tau_{6\text{db}}$ satisfies the following equation:

$$\frac{2A}{T_e^2}\left(\frac{\tau_{6\text{db}}}{2}\right)^2 = 6. \tag{63}$$

Then we obtain

$$\tau_{6\text{db}} = \sqrt{\frac{12}{A}}\,T_e = \sqrt{\frac{12}{A}}\,\frac{V_0}{v_e}. \tag{64}$$

If we use the half-amplitude voltage width $V_{6\text{db}}$ of the output pattern $A(V)$ in place of V_0, (57) and (64) are rewritten as

$$A(V) = G\cdot\exp\left[-(\ln 2)\left(\frac{2V}{V_{6\text{db}}}\right)^2\right] \tag{65}$$

$$\tau_{6\text{db}} = \frac{V_{6\text{db}}}{v_e} \tag{66}$$

because

$$\frac{A}{12} = \left(\frac{V_0}{V_{6\text{db}}}\right)^2. \tag{67}$$

Note that the half-amplitude duration of the output pulse is proportional to the reciprocal of the helix voltage sweep velocity. This is a special case in which the presence of the helix delay time does not affect the shape of the output pulse. On the other hand peak or average power of the output pulse is affected severely with the helix delay time.

Summarizing the characteristics of the output pulse, we obtain the following:

pulse shape, Gaussian,
modulation delay $T_g/2$,
half-amplitude duration,

$$\tau_{6db} = \sqrt{\frac{12}{A}}\frac{V_0}{v_e} = \frac{V_{6db}}{v_e},$$

relative value of peak power P_p,

$$10 \log_{10} P_p = -2\left(\frac{T_g}{\tau_{6db}}\right)^2 = -\frac{A}{6}\left(\frac{T_g}{T_e}\right)^2, \qquad (68)$$

relative value of average or total power P_N

$$10 \log_{10} P_N = 10 \log_{10} \tau_{6db} - 2\left(\frac{T_g}{\tau_{6db}}\right)^2$$

$$= 10 \log_{10}\left(\sqrt{\frac{12}{A}} T_e\right) - \frac{A}{6}\left(\frac{T_g}{T_e}\right)^2. \qquad (69)$$

P_p and P_N/T_g are calculated and illustrated in Figs. 22 and 23 as a function of (τ_{6db}/T_g). These curves show the variation of peak or average power as a function of τ_{6db} when T_g is held constant.

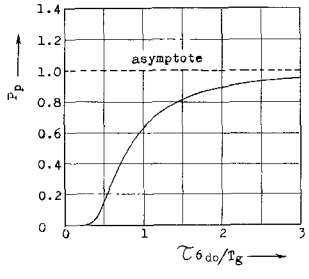

Fig. 22—P_p vs τ_{6dB}/T_g.

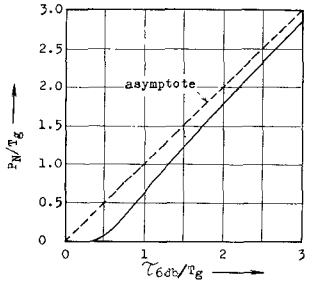

Fig. 23—P_N/T_g vs τ_{6dB}/T_g.

Appendix IV

Interferometer Application for Measuring Half-Amplitude Duration of Repetitive Carrier Pulses[1]

Application of the interferometer generally found in the literature is concerned with the measurement of autocorrelation function. It was found in this experiment that the half-amplitude duration of repetitive carrier pulses can be measured with the same device. The construction of the interferometer used here is sketched in Fig. 24.

A feature of this device is that a larger time constant of the detector is used than in the usual interferometer.

Here, the time constant is selected sufficiently larger than the period of the pulse train to be measured.

The detector input is an amplitude sum of two pulse trains having the identical envelope forms, one of which is delayed by the delay time τ with respect to the other.

The detector output is a function of the peak amplitude of the input. This function is linear when the detector behaves as a large signal one, and approximately quadratic when the detector behaves as a small signal one. It was found that the detector used in this experiment behaves as a quadratic peak detector because the input level was small.

If we increase τ slowly, the detector output is obtained as a function of τ as illustrated in Fig. 25.

It is easily seen that the edges of the output pattern in Fig. 25 correspond to such τ that the half-amplitude points of two pulses just coincide.

Then, it is concluded that the width of the interferometer output pattern D is twice the half-amplitude duration of the original pulses τ_{6db}.

$$D = 2\tau_{6db}. \qquad (70)$$

Eq. (70) is valid only for repetitive pulses without long residual tails. An example is illustrated in Fig. 26 to show how the width of the interferometer output becomes larger than twice the half-amplitude duration of pulses if long residual tails are present.

If the envelope of the original pulse and the characteristic of the detector are known, we can make use of D_t illustrated in Fig. 26 instead of D in order to obtain the half-amplitude duration. Calculations in [5] show that D_t is nearly equal to τ_{6db} when the pulse envelope is Gaussian and the detector is a quadratic peak detector.

The interferometer pattern is always symmetrical with respect to its center. If the measured pattern shows asymmetry, there is waveform distortion present in one of its arms.

[1] The waveguide interferometer used in this experiment has been designed by F. Ishihara. The details of this appendix are to be published in another paper [5].

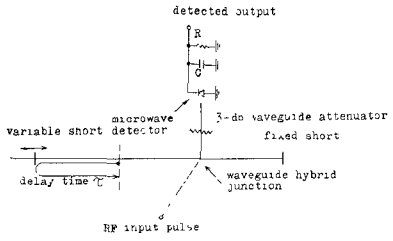

Fig. 24—Construction of waveguide interferometer.

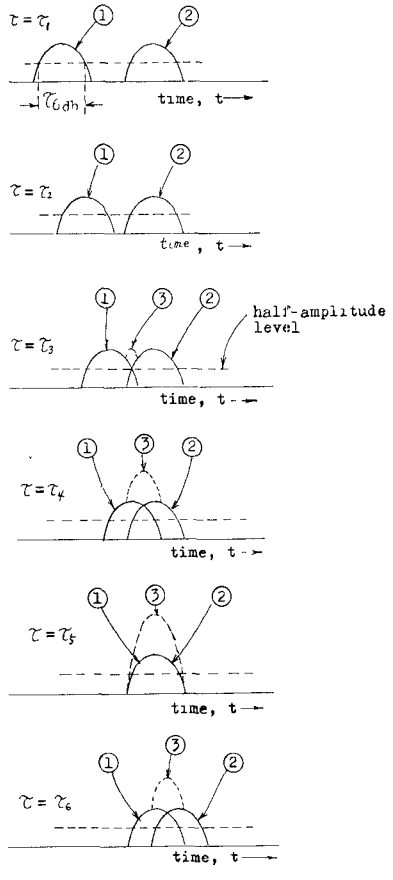

Fig. 25—Superposed envelopes of pulses and interferometer output as a function of delay time.
①: Envelope of pulse having variable delay.
②: Envelope of pulse having fixed delay.
③: Envelope of superposed two pulses.

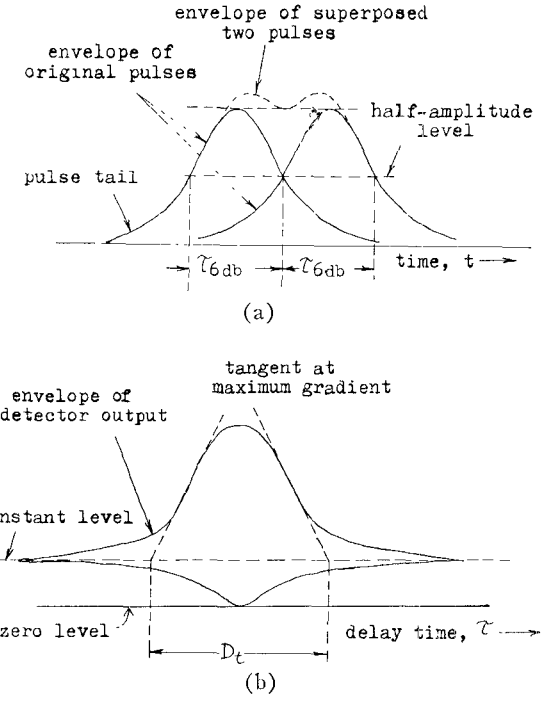

Fig. 26—Superposed envelope of pulses and interferometer output when pulse to be measured has long residual tails.

An advantage of the interferometer described here is that it does not require a large output frequency band of the microwave detector. This makes the design of the detector easy and affords a measuring method of very short pulses with high repetition rate.

Acknowledgment

The author is indebted to the staff of the Electrical Communication Laboratory, and especially to Dr. B. Oguchi and F. Ishihara for their encouragement and many suggestions during this investigation.

References

[1] W. A. Klute, "Pulse generation and shaping at microwave frequencies," *Bell. Labs. Record*, vol. 29, pp. 216–220; May, 1951.
[2] A. C. Beck and G. D. Mandeville, "Microwave traveling-wave tube millimicrosecond pulse generators," IRE Trans on Microwave Theory and Technique, vol. MTT-3, pp. 48–51; December, 1955.
[3] M. Tsuchiya and K. Iwata, Internal Rept. of Electrical Communication Laboratory, Nippon Tel. and Tel., Tokyo, Japan, Keika-Shiryo No. 543; May, 1957.
[4] Y. Nakamaru, H. Tsuru and A. Saheki, Record of The Institute of Electrical Communication Engineers of Japan Annual Conference, Tokyo, Japan, No. 1273, 1960.
[5] F. Ishihara, "Measurements of RF Pulse with an Interferometer," (to be published).
[6] R. C. Cumming, "The serrodyne frequency translator," Proc. IRE, vol. 45, pp. 175–186; February, 1957.
[7] J. R. Pierce, "Traveling-Wave Tubes," D. Van Nostrand Co., Inc., New York, N. Y., pp. 125–126; 1950.
[8] T. Miwa, J. Koyama, M. Mishima, and I. Yanaoka, "Helix Type Traveling-Wave Tube for 24 Gc/s," Travaux du Congrès International Tubes Hyperfrequencies, Paris, France, Conservatoire National des Arts et Métiers, Paris, p. 554; 1956.